Revealing temperature-dependent polymer aggregation in solution with small-angle X-ray scattering†

Maged Abdelsamie, ‡[ab] Thomas P. Chaney, ‡[c] Hongping Yan,[ad] Sebastian A. Schneider,[ae] I. Alperen Ayhan,[f] Enrique D. Gomez,[fg] John R. Reynolds [h] and Michael F. Toney *[aci]

Improving the morphology of bulk heterojunction active layers remains a primary challenge for organic photovoltaics (OPVs), and much research has been devoted to achieving this through modifying OPV casting solutions to control film formation and crystallinity. Yet, the solution conformation of conjugated polymers used in OPVs is largely unknown. Here, we report observations of temperature dependent aggregation (TDA) through small-angle X-ray scattering (SAXS) investigations of polymer conformation in chlorobenzene : dichlorobenzene casting solvent as a function of temperature for PffBT4T-2OD, a polymer known to display TDA, and its derivative PffBT3T-2OD which displays significantly reduced TDA. We find that, upon cooling below 80 °C, PffBT4T-2OD forms large crystalline aggregates in solution, while its derivative PffBT3T-2OD forms mostly amorphous aggregates of similar size with some evidence of short-range order. This change in solution aggregation behavior is reflected in the lack of gelation by PffBT3T-2OD upon film deposition by spin coating. Grazing-incidence wide-angle X-ray scattering (GIWAXS) revealed a preferred face-on $\pi-\pi$ stacking orientation for PffBT3T-2OD films while PffBT4T-2OD's $\pi-\pi$ stacking peak was isotropic. We combine these findings to suggest that the presence of crystalline seed aggregates in PffBT4T-2OD solution quickly form an isotropic crystallite network upon cooling while PffBT3T-2OD's amorphous aggregates more slowly crystallize resulting in improved processability of PffBT3T-2OD.

1. Introduction

The active layer morphology in organic photovoltaics (OPVs) has been shown to be a dominant effect on device efficiency.[1,2] This is because several key processes take place within the active layer. First, energy from light is absorbed to create an exciton. This exciton must then diffuse to an interface between donor and acceptor molecules in order to split into charge carriers. However, excitons are short lived states and can only diffuse ~10 nm before decaying through radiative and non-radiative pathways.[3] Upon the exciton diffusion to the donor/acceptor interface, it dissociates into a charge transfer state, followed by separation of charges into free charge carriers (electrons and holes).[4] After separation, these charge carriers then need to find a path through the donor and acceptor to their respective electrodes. These processes put strict constraints on the morphology of OPV active layers. They must consist of small domain sizes (10–20 nm) so that all generated excitons can diffuse to an interface to be split. The donor and acceptor domains must also be bi-contiguous such that each charge can find its way to the electrode. Finally, it is thought that pure and crystalline domains increase charge carrier mobility and more efficiently extract the generated charges. Control of this morphology remains the crucial challenge in improving OPV performance.

Many strategies have been developed to better control the morphology of OPV active layers such as solution shearing,[5] solvent additives,[6] high deposition temperatures,[7] and chemical

[a]Stanford Synchrotron Radiation Lightsource, SLAC National Accelerator Laboratory, Menlo Park, CA, 94025, USA

[b]Materials Sciences Division, Lawrence Berkeley National Laboratory, Berkeley, CA, 94720, USA. E-mail: Michael.Toney@colorado.edu

[c]Materials Science and Engineering, University of Colorado, Boulder, CO 80309, USA

[d]Department of Chemical Engineering, Stanford University, Stanford, CA, 94305, USA

[e]Department of Chemistry, Stanford University, Stanford, CA, 94305, USA

[f]Department of Chemical Engineering, The Pennsylvania State University, University Park, PA 16802, USA

[g]Department of Materials Science and Engineering, The Pennsylvania State University, University Park, PA 16802, USA

[h]School of Chemistry and Biochemistry, School of Materials Science and Engineering, Center for Organic Photonics and Electronics, Georgia Tech Polymer Network, Georgia Institute of Technology, Atlanta, GA, 30332, USA

[i]Department of Chemical and Biological Engineering, Renewable and Sustainable Energy Institute (RASEI), University of Colorado, Boulder, CO 80309, USA

† Electronic supplementary information (ESI) available. See DOI: 10.1039/d1ta09086k

‡ Both authors contributed equally.

modification.[8] A large component of these strategies is controlling the level of aggregation of OPV polymers in solution. Aggregates in solution have largely been reported to be beneficial for OPV device efficiency,[9–14] yet in some cases too much solution aggregation can be detrimental.[11,15,16] No clear consensus has been reached regarding the optimal solution behavior of OPV polymers. On one hand, aggregates can serve as nucleation sites creating pure, crystalline domains that have high charge extraction efficiencies, but aggregates can also result in large domain sizes within the film limiting exciton splitting. A comprehensive understanding of conjugated polymer conformations in differing degrees of solvation is necessary to understand both solution aggregation and resulting film morphology. This understanding may then be used to control morphology through changes to polymer and solvent chemistries and the polymer–solvent interactions. This study utilizes small angle X-ray scattering (SAXS) to elucidate polymer conformations in solution.

There has been a limited number of previous studies investigating polymer–solvent interactions for conjugated polymers with somewhat differing conclusions depending on the solvent and polymer. Small angle neutron scattering experiments by McCulloch *et al.*[17] indicated that poly(3-hexylthiophene-2,5-diyl) (P3HT) is well-solvated in 1,2-dichlorobenzene (oDCB) through observations of a Porod region that scales with $\sim q^{-2}$ which shows the chains exhibit an expanded coil conformation. Conversely, studies by Schmidt *et al.*[18] found evidence for collapsed coils conformation and aggregation of PDPP2FT-C16 in chlorobenzene (CB) solutions with the additive 1-chloronapthalene (CN). In solutions containing CN, a secondary Porod region indicating stiff chains along with a broad lamellar diffraction peak was observed. Additionally, Brady *et al.*[19] used solution SAXS to investigate aggregation upon cooling in another diketopyrrolopyrrole containing polymer, DPPT-T, in neat oDCB. Similar evidence of aggregation was found through the emergence of a secondary Porod region suggestive of stiff chain conformation and a weak diffraction peak near the expected lamellar stacking spacing. While P3HT is well-solvated in chlorinated aromatic solvents, polymers containing non-thiophene moieties, including but not limited to diketopyrrolopyrrole units, have demonstrated propensity for solution aggregation.

One high performing OPV polymer that exhibits a strong tendency to aggregate is PffBT4T-2OD[11,12,20] which has achieved PCEs over 10%.[21] However, a major issue with this and other high performing donor polymers is the requirement of strict processing parameters to form optimal morphology. In the case of PffBT4T-2OD in a CB : oDCB casting solvent, solution aggregates quickly form a gel and prevent film deposition at room temperature conditions.[21] To solve this problem, Xu *et al.*[21] demonstrated that by simply removing a thiophene from the PffBT4T-2OD repeat unit, creating PffBT3T-2OD, crystalline aggregation was strongly suppressed as evidenced by UV-vis measurements. Because of this, PffBT3T-2OD demonstrates enhanced processability where it can be deposited easily as a uniform film at room temperature, unlike its counterpart PffBT4T-2OD. Additionally, Xu *et al.* showed films prepared from copolymers with varying ratios of PffBT4T-2OD and PffBT3T-2OD monomers experienced little change in UV-vis absorption profiles and hole mobility indicating that the optoelectronic properties in the solid were not altered from neat PffBT4T-2OD. At the same time, the reason behind the higher solubility and reduced gelation of the PffBT3T-2OD polymer compared to PffBT4T-2OD continues to be a question.

In this work, we compare the solution behavior of the highly aggregating PffBT4T-2OD to its derivative, PffBT3T-2OD, which we show to have no crystallinity in CB : oDCB solution leading to greatly improved processability. To elucidate the mechanism behind the increased processability of PffBT3T-2OD, SAXS and dynamic light scattering (DLS) was used on PffBT4T-2OD and PffBT3T-2OD in solution at various temperatures to observe the characteristics of aggregate formation in each polymer. Models were fit to the resulting X-ray scattering profiles elucidating the presence of polymer aggregates on the order of 10 s of nanometers in both polymers at all temperatures. Through analyzing the scaling of Porod regions along with the emergence of lamellar diffraction peaks, it was found that PffBT4T-2OD, upon cooling, exhibits defined crystalline aggregates, which was corroborated by DLS measurements. This behavior contrasts with PffBT3T-2OD, which remained largely amorphous down to room temperature. It is the presence of these crystalline aggregates in solution which result in gelation through the formation of crystallite networks.

2. Results and discussion

2.1 Effect of temperature on the aggregation of PffBT4T-2OD and PffBT3T-2OD in solution

PffBT4T-2OD and PffBT3T-2OD polymers were synthesized by Migita–Kosugi–Stille polymerization as described in literature[21] resulting in number average molecular weights/dispersities of 43.9 kDa/2.05 and 60.4 kDa/1.75, respectively. The polymers were dissolved in 1 : 1 mixture of oDCB and CB then flowed through a capillary where SAXS measurements were taken over a temperature range from 80 to 20 °C (Fig. S1†). Line profiles, with neat solvent contribution subtracted, were constructed through azimuthal integration over a 100° sector and are shown in Fig. 1a and c (additional line profiles shown in Fig. S2 and S3†), while the corresponding 2D SAXS plots are shown in Fig. 1b and d (additional 2D plots in Fig. S4 and S5†) for PffBT4T-2OD and PffBT3T-2OD samples, respectively. For PffBT4T-2OD, no indication of diffraction peaks is present at 80 °C (Fig. 1a and S4a†). However, upon cooling to 65 °C, a sharp peak at ≈ 0.24 Å^{-1} was observed and found to strengthen in intensity as the temperature decreases further (Fig. 1a, b and S4b–d†). This peak likely results from lamellar stacking due to close similarity with the lamellar *d*-spacings measured in PffBT4T-2OD films.[21] Additional observation of TDA behavior in PffBT4T-2OD was made through DLS experiments. When cooled to low temperatures, the emergence of a population of larger aggregates was observed in the PffBT4T-2OD solution alongside a secondary smaller diameter population as shown in Fig. S6.† DLS measurements were taken at several angles and the dominant decay rate as a function of

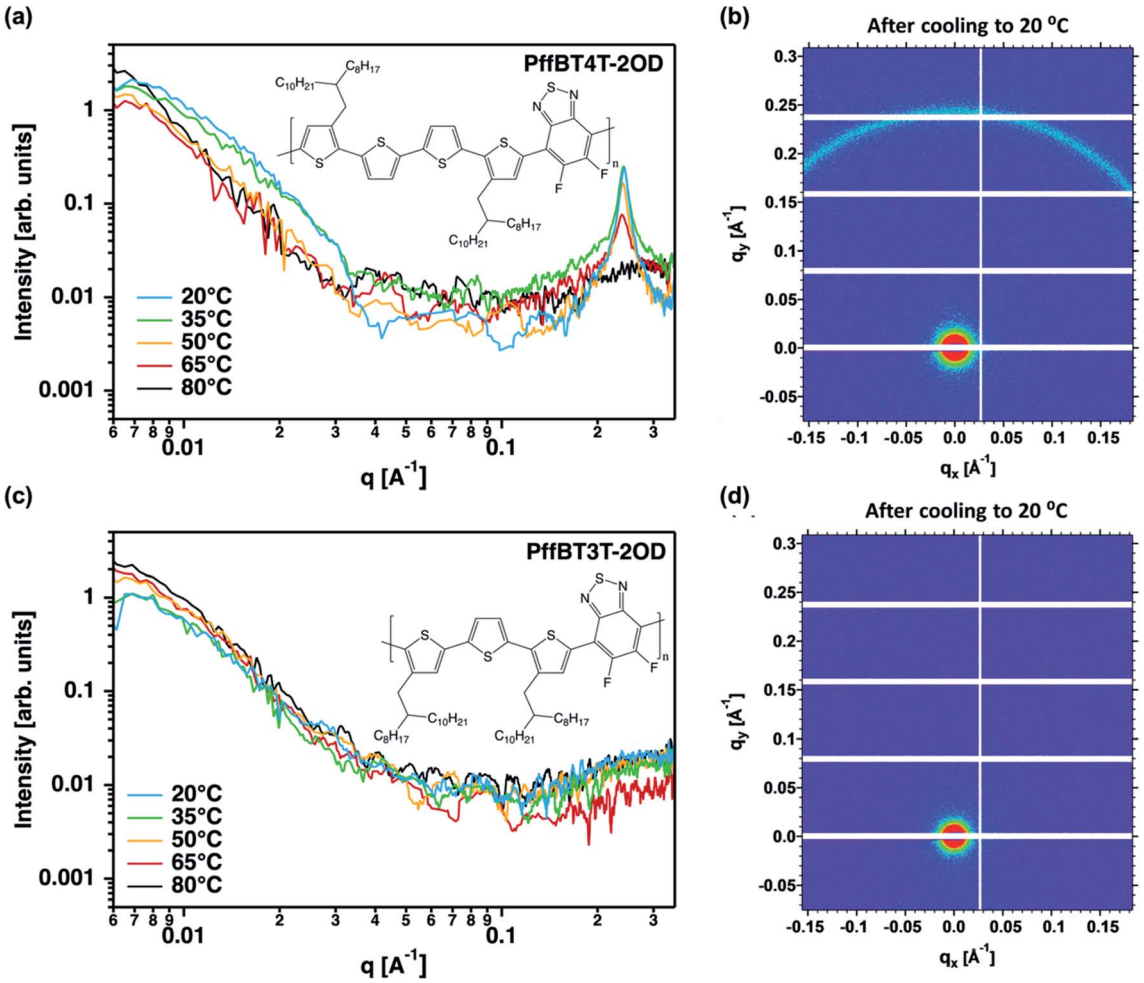

Fig. 1 Solution small-angle X-ray scattering (SAXS) 1D profiles for (a) PffBT4T-2OD and (c) PffBT3T-2OD in a solvent mixture of oDCB : CB [1 : 1] at different temperatures (20 to 80 °C). At q > 0.02 Å^{-1} intensity values were smoothed with 10 point moving average to reduce the noise. 2D plots taken at 20 °C are shown for PffBT4T-2OD and PffBT3T-2OD in (b) and (d) respectively.

collection angle was fit to a linear relation giving the diffusion coefficient which is used to find the hydrodynamic size.[22] DLS data is included in Fig. S7 and S8.†

In contrast, there is no distinct diffraction peak in the PffBT3T-2OD SAXS data at any temperature demonstrating a lack of crystalline aggregation (Fig. 1c, d and S5†). This is consistent with previous UV-vis measurements[21] along with observations of the low solubility of PffBT4T-2OD compared with PffBT3T-2OD. However, a weak, broad peak is observed in the PffBT3T-2OD sample across all temperatures. This peak, also centered about 0.24 Å^{-1}, is suggestive of a short-ranged lamellar association similar to those observed in diketopyrrolopyrrole based polymers.[18,19] To gain more insights into the differing solution behavior of PffBT4T-2OD and PffBT3T-2OD, the SAXS 1D data was fit against a model.

2.2 Model fits of solution SAXS profiles for PffBT4T-2OD and PffBT3T-2OD

To obtain more quantitative insight in polymer molecular conformation, modeling for these data was carried out using the Igor Irena program.[23] Lorentzian curves were used to model the diffraction peaks at high q (>0.06 Å^{-1}) and a unified scattering function combining Guinier and Porod behavior developed by Greg Beaucage (eqn (S1)†)[24,25] was used to model the low q region (<0.06 Å^{-1}).

As shown in Fig. 1, the PffBT4T-2OD sample displayed a sharp diffraction peak in the high q range upon cooling attributed to the emergence of lamellar stacking in aggregates. However, close examination of the data and the shape of this peak indicates it is composed of two superimposed Lorentzian curves as presented in Fig. 2. We categorize these two peaks as broad and narrow. The broad peak is found to appear in both PffBT4T-2OD and PffBT3T-2OD at all temperatures and the narrow peak only appears in the PffBT4T-2OD solution at temperatures of 65 °C and below. The concurrent presence of these two peaks suggests two distinct polymer conformations are taking place.

The narrow peak is indicative of crystalline aggregates within solution. It is centered about a $q = 0.24$ Å^{-1} and corresponds to a d-spacing of 2.6 nm which is larger than reported lamellar

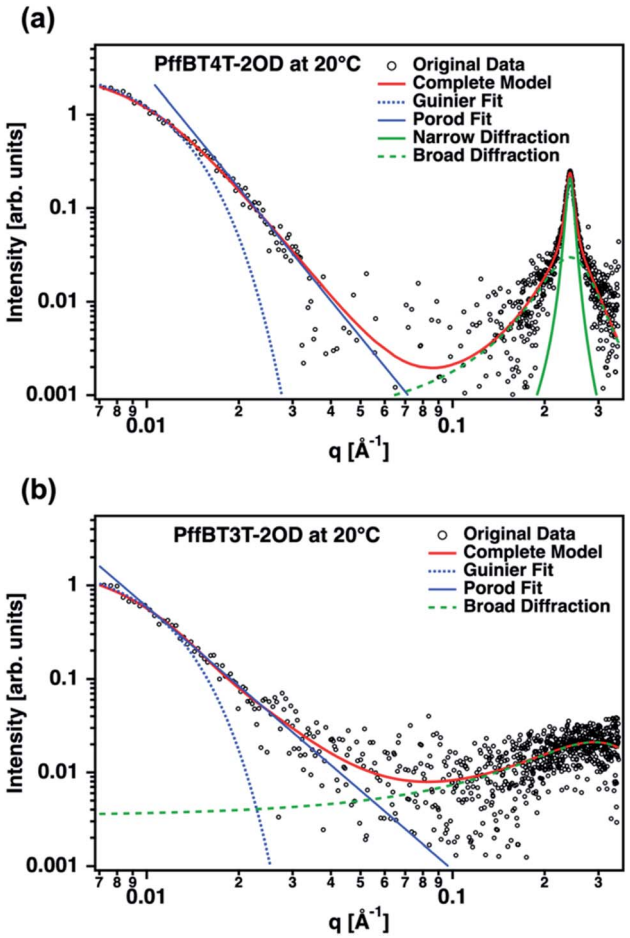

Fig. 2 Solution small-angle X-ray scattering (SAXS) profiles and their fits for PffBT4T-2OD and PffBT3T-2OD in a solvent mixture of oDCB : CB [1 : 1] at 20 °C in (a) and (b), respectively. The low q range in (a) and (b) was fitted with a unified fit model that relies on combination of Porod's and Guinier's law. The high q range in (a) was fitted using Lorentzian curves.

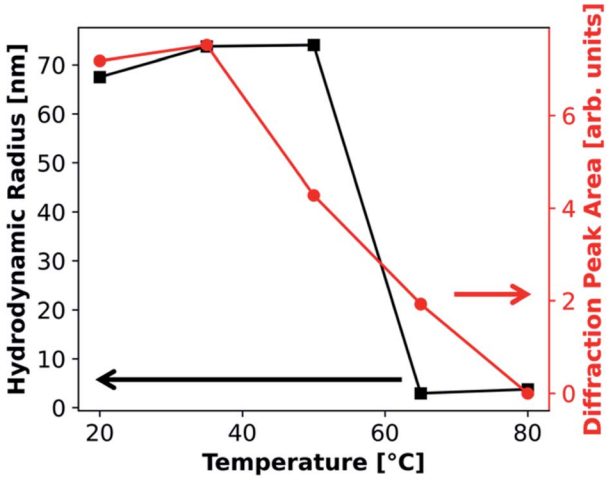

Fig. 3 Hydrodynamic radius reported from DLS measurements and narrow diffraction peak area reported from solution SAXS measurements as a function of temperature for PffBT4T-2OD. Similar transitions around 50 °C from both measurements demonstrate temperature dependent aggregation.

stacking distance of 2.1 nm for PffBT4T-2OD films. This difference suggests that the lamellae in solution are likely swollen with solvent. Previous studies have shown a decrease in lamellar spacing upon solvent removal during film formation for different polymers such as PCPDTBT[26] and pDPP.[27] Upon cooling, the peak increases in intensity and shifts slightly towards larger q values which can be explained through an increase in aggregation along with deswelling of the lamellae through diminished polymer–solvent interactions. We can use the integrated peak intensity as a measure of the relative total amount of aggregated material within the solution. Fig. 3 shows the temperature dependence of the integrated scattering intensity of the narrow peak. A clear transition takes place during cooling from 65 °C to 35 °C where the aggregated fraction of polymer increases dramatically. This data was supported by DLS measurements which showed a sharp increase in hydrodynamic radius upon cooling below 65 °C shown in Fig. 3. This is consistent with TDA behavior of PffBT4T-2OD reported previously.[11] Thus, we attribute the appearance of the narrow diffraction peak in PffBT4T-2OD with the formation of large solution aggregates featuring long-range lamellar ordering; we hypothesize that these aggregates also have ordered π–π stacking that may drive the lamellar ordering, but the π–π stacking peak is outside of our data range and may be too weak to observe.

The average narrow peak FWHM of 0.016 Å^{-1} in PffBT4T-2OD solutions give a correlation length of 38.5 nm through a Scherrer relation. This is possibly related to crystallite size but could also be attributed to cumulative disorder and paracrystallinity.[28] The absence of a strong lamellar stacking peak, and therefore crystalline aggregates, in the PffBT3T-2OD solution fits well with observations of increased solubility and improved room temperature film formation.[21]

Accurate fitting of the broad peak was made difficult due to the weak intensity and the detector cutoff at 0.35 Å^{-1}. However, average FWHM were able to be estimated at 0.17 Å^{-1} and 0.34 Å^{-1} for PffBT4T-2OD and PffBT3T-2OD respectively with a corresponding correlation length of a few nanometers. The small extent of order suggests the origin of the peak is likely a near neighbor association and no evidence of extended order. While the broad peak is centered near the lamella packing q value for PffBT4T-2OD and PffBT3T-2OD, it is unlikely that the structures producing it are contributing to temperature dependent aggregation due to its small coherence length and presence at all temperatures.

The low q regime was fit using a unified model composed of Guinier and Porod equations.[24,29] The Guinier equation fits the low q behavior and is related to aggregate size while the Porod equation describes the sharpness of the interface of scatterers. From this model, the radius of gyration (R_g) and Porod exponent were extracted and reported in Fig. 4. There was little systematic variation found in the R_g values of PffBT4T-2OD and PffBT3T-2OD across the temperature range with average values of

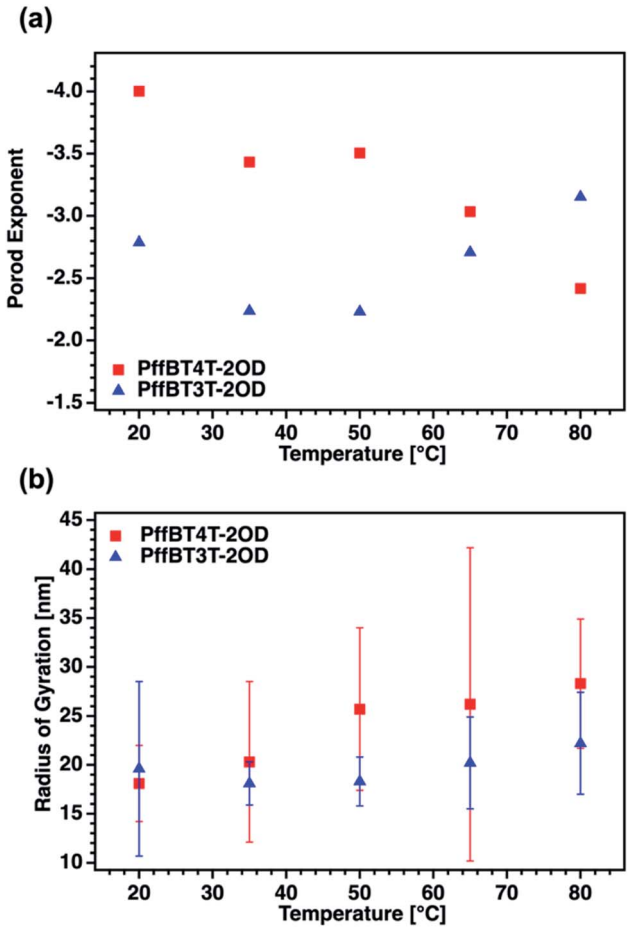

Fig. 4 Porod exponents (a) and radius of gyration values (b) extracted from model fits for PffBT4T-2OD and PffBT3T-2OD SAXS profiles. We were unable to calculate error bars for the Porod exponent due to high noise level in the data.

24 nm and 20 nm respectively. However, the low-q cutoff limited accurate determination of R_g values as shown by the large error bars. Despite this limitation, we are still able to draw the following conclusions. Utilizing the calculated persistence length of 3.7 nm for PffBT4T-2OD,[30] a single PffBT4T-2OD polymer chain is expected to have an $R_g \approx 9$ nm from the worm-like chain model.[31] Therefore, R_g values greater than 20 nm points towards aggregation of multiple polymers in both PffBT4T-2OD and PffBT3T-2OD. An R_g of 24 nm matches well to the Scherrer estimation of PffBT4T-2OD domain sizes of 38.5 nm suggesting that below 65 °C PffBT4T-2OD aggregates are composed primarily of crystalline polymer.

The differences between hydrodynamic radius reported by DLS (70 nm for PffBT4T-2OD at 20 °C) and radius of gyration reported by solution SAXS (18 nm for PffBT4T-2OD at 20 °C) is attributed to differing experimental parameters between the two measurements. Due to the highly absorbing nature of PffBT4T-2OD, DLS measurements were limited to solution concentrations two orders of magnitude lower than SAXS measurements. Other studies of conjugated polymers have demonstrated a similar drastic increase in DLS measured aggregate size at concentrations below 1 mg mL^{-1}.[32,33]

It is important to note that PffBT3T-2OD is shown, from solution SAXS, to be aggregating to nearly the same size as PffBT4T-2OD without any evidence of long-range order. Despite forming large aggregates, PffBT3T-2OD does not demonstrate the same gelling at low temperatures as PffBT4T-2OD. The difference in the nature of aggregation for each of these polymers is further demonstrated through the Porod exponent shown in Fig. 4. In PffBT4T-2OD, the Porod exponent decreases upon cooling from −2.5 to −4 indicating a change from a clustered network of polymers to a more solid, defined aggregate exhibiting surface fractals. This densification is concurrent with the appearance of the narrow diffraction peak signifying the PffBT4T-2OD chains collapse from a loose amorphous aggregate at 80 °C into a compact highly crystalline aggregate upon cooling. No evidence of temperature dependence with Porod exponent was observed in the PffBT3T-2OD solution likely because no crystallization, and therefore no densification, takes place upon cooling.

2.3 GIWAXS measurements of PffBT4T-2OD and PffBT4T-2OD thin films

To understand the molecular packing in thin films, grazing-incidence wide-angle X-ray scattering (GIWAXS) was performed on neat films of PffBT4T-2OD and PffBT3T-2OD coated from CB : oDCB [1 : 1]. 2D GIWAXS patterns and the scattering intensities of the films integrated over a chi range of 0°–90° are shown in Fig. 5. PffBT4T-2OD shows scattering from lamellar stacking centered at $q \sim 0.3$ Å^{-1} and scattering from π–π stacking centered at $q \sim 1.78$ Å^{-1}, and these peaks are assigned to the (100) and (010) reflections, respectively, see Fig. 5a and c. 2D GIWAXS pattern of PffBT3T-2OD shows lamellar and π–π stacking scattering centered at $q \sim 0.26$ Å^{-1} and $q \sim 1.77$ Å^{-1}, respectively, as shown in Fig. 5b and c. While PffBT3T-2OD exhibits larger lamellar spacing values of $d_{100} \sim 24$ Å compared to ∼21 Å for PffBT4T-2OD consistent with previous reports.[12,21] Both polymers exhibit similar π–π stacking spacing of $d_{010} \sim 3.5$ Å. As mentioned earlier, PffBT4T-2OD films exhibit decrease in lamellar spacing compared to PffBT4T-2OD crystallites in solution confirming the densification of PffBT4T-2OD crystallites in thin films. The scattering patterns reveals distinct differences in crystallite orientation between the two polymers as evidenced by pole figures – plots of intensity *vs.* polar angle – included in Fig. S9.† The (010) π–π stacking peak is more localized in the out-of-plane direction for PffBT3T-2OD films indicating a more dominant face-on orientation, whereas the (010) π–π stacking peak for PffBT4T-2OD exhibits more isotropic orientation. It is worth noting that these orientation preferences are affected by the processing conditions. For instance, previous work[21] has shown a more preferred face-on orientation for both polymers in neat films when they were cast from pure CB on substrates at a lower temperature.

2.4 Mechanism of temperature-dependent aggregation

PffBT4T-2OD has been shown to exhibit relatively dense and highly crystalline aggregates in solution below 65 °C compared to largely amorphous aggregates exhibited in PffBT3T-2OD

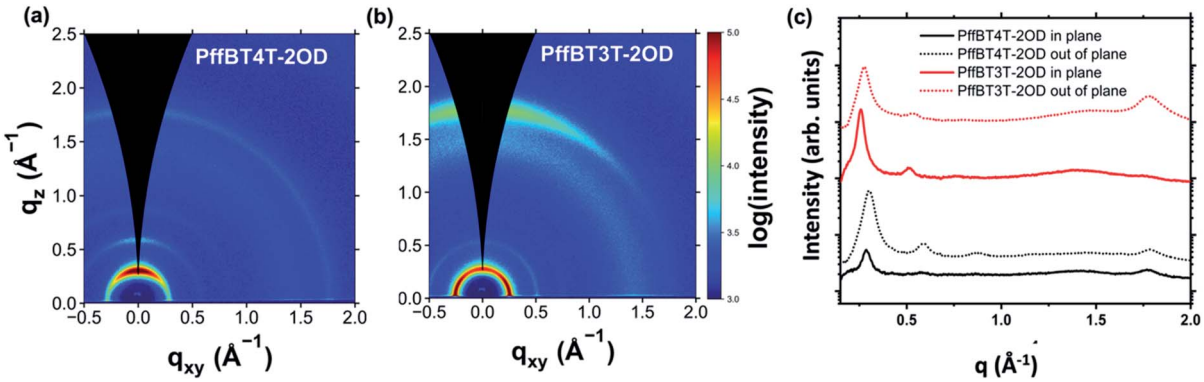

Fig. 5 2D GIWAXS images of polymer thin films; (a) PffBT4T-2OD and (b) PffBT3T-2OD. (c) Integrated scattering intensity of GIWAXS measurements shown in (a) and (b).

solutions. The differences in solution aggregation of these two similar polymers is reflected by their gelation during film formation; PffBT4T-2OD rapidly gels at room temperature preventing the development of a uniform film while PffBT3T-2OD does not have these problems. First, we examine the mechanism behind the formation of aggregates in solution with a casting solvent. It has been shown that the aggregation behavior of the PffBT4T class of polymers is sensitive to the branching point position on alkyl sidechains with branching close to the backbone presenting a barrier to the formation of crystalline aggregates.[11,13] The second carbon position of the sidechain branching in PffBT4T-2OD presents a moderate steric hinderance between side chains that prevents crystallization in solution at high temperatures, but this steric hinderance is overcome at lower temperatures allowing for crystallization.[11] For PffBT3T-2OD, there is one less thiophene per repeat unit which effectively increases the density of the branched sidechains. This results in greater steric hinderance caused by the sidechains and prevents crystalline aggregation in solution at all temperatures.

As the PffBT4T-2OD and PffBT3T-2OD solutions cool, the presence or absence of crystalline aggregates determines the extent of gelation. For PffBT4T-2OD, there is a low thermodynamic nucleation barrier due to the presence of crystalline aggregates which act as seed nuclei. Upon film deposition, this allows for the existing aggregates to rapidly form a network, as schematically illustrated in Fig. 6, and trap the remaining solvated polymer preventing liquid-like flow. In contrast,

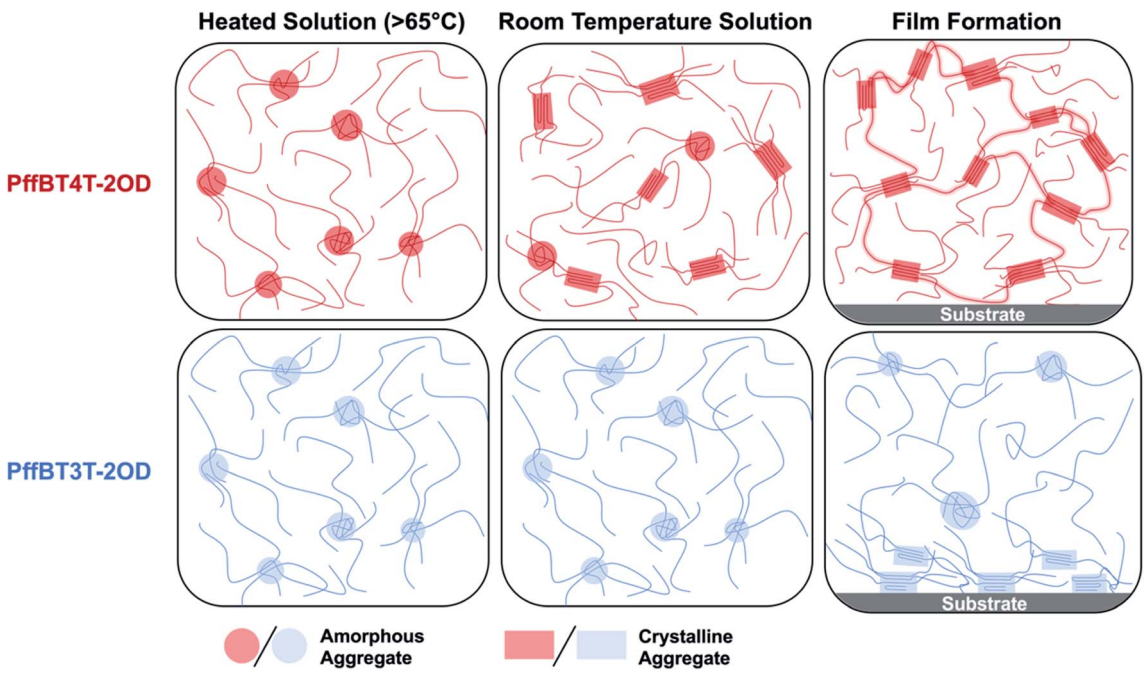

Fig. 6 Schematic representation of polymer aggregation in heated solutions, room temperature solutions, and upon film formation. In heated solutions, both PffBT4T-2OD and PffBT3T-2OD form amorphous aggregates. Upon cooling to room temperature, the PffBT4T displays crystalline aggregates which quickly forms a gelled network through tie chains upon film formation. PffBT3T however, does not from crystalline aggregates in solution and instead relies on crystallite nucleation at the substrate resulting in greater crystallite alignment.

PffBT3T-2OD, having only formed amorphous aggregates, cannot quickly form such a network due to a high thermodynamic nucleation barrier to connecting aggregates *via* crystallization. Instead, crystallization likely nucleates at the substrate interface resulting in the preferred face-on orientation seen in GIWAXS measurements.

3. Conclusion

To conclude, we have observed temperature dependent aggregation in PffBT4T-2OD polymer solutions through SAXS measurements. We found that long-range crystalline order with domain sizes on the order of tens of nanometers appears within the aggregates of PffBT4T-2OD when cooled to 65 °C and below. No such long-range order appears in the slightly modified polymer PffBT3T-2OD, but through data modeling, it is shown that both polymers exhibit aggregate sizes near 20 nm. Thus, importantly, the increased processability of PffBT3T-2OD is attributed not to a smaller aggregate size, but rather a reduction in solution aggregate crystallinity. Upon cooling, it is hypothesized that PffBT4T-2OD rapidly connects crystallite aggregates present in solution to produce a gel resulting in no preferred orientation. PffBT3T-2OD, possessing only amorphous aggregates, crystallizes more slowly resulting in a preferred face on orientation shown by GIWAXS measurements. Therefore, the simple chemical modification of the PffBT4T-2OD monomer structure to PffBT3T-2OD greatly improves solution processability through reducing aggregate crystallinity.

4. Experimental section

4.1 Materials and solution preparation

PffBT4T-2OD and PffBT3T-2OD were synthesized following published procedures.[34,35] The neat polymers were dissolved at a concentration of 5 mg mL^{-1} for solution SAXS and 0.05 mg mL^{-1} for DLS in a solvent mixture of 1,2-dichlorobenzene (oDCB) : chlorobenzene (CB) [1 : 1] at 110 °C for at least 3 h. For solution SAXS, the pre-heated solution at 110 °C was injected into pre-heated capillary tube at 80 °C. For DLS the preheated solution was placed into a pre-heated measurement vial. To prepare thin films, preheated solution at 110 °C was dropped on preheated substrates at 110 °C and spin coated at 800 rpm for 60 s, where the substrates and solution cool down by convection during spin coating.

4.2 Solution small-angle X-ray scattering (SAXS)

Solution SAXS was collected at beamline 4–2 at the SSRL. The setup used for measuring solution SAXS is represented in Fig. S1.† The solution sample was contained in quartz capillary tube with a 1 mm diameter and 0.1 mm wall thickness, purchased from the Charles Supper Company, Inc. The Capillary tube was placed in a metal holder connected to a heating/cooling element to control the solution temperature. The capillary tube was connected to polyvinylidene fluoride fluoropolymer (PVDF) tubing for solution injection. To avoid gelation, solutions were heated to 110 °C prior to injection into the capillary tube. 60 one-second detector exposures were collected at 80 °C and at every 15 °C cooling step down to 20 °C. Exposures were taken with static solution and the setup was allowed ~5 minutes to equilibrate at each temperature prior to measurement. X-ray energy of 15 keV was used, with a sample-detector distance of 3.5 m. Pilatus 1 M fast detector was used to collect the scattered X-rays. Scattering background from pure solvents (CB : oDCB [1 : 1]) was acquired using the same exposure times and cooling profile as the solution measurements. The pure solvent background was subtracted from the precursor solution SAXS profiles collected at matching temperatures to give the scattering contribution from only the polymer.

4.3 Grazing incidence wide-angle X-ray scattering (GIWAXS)

GIWAXS was performed at the Stanford Synchrotron Radiation Lightsource (SSRL). GIWAXS measurements were obtained at beamline 11–3 at an X-ray energy of 12.7 keV using an incident angle of 0.13°. The sample-to-detector distance was calibrated using a LaB_6 standard and was 341.2 mm. Data processing was performed using the Nika software package for Wavemetrics Igor,[36] in combination with WAXStools,[37] with a custom written Igor script.

4.4 Dynamic light scattering (DLS)

DLS measurements were performed on the polymer solutions at various temperatures (cooling from 80 °C to 20 °C) using a Brookhaven Instruments BI-200 SM static/dynamic light scattering system equipped with a 30 mW diode laser ($\lambda = 538$ nm). Particle size distributions were determined at various scattering angles ranging from 30° to 90°. Diffusion coefficients in chlorobenzene were determined from the slope of the linear relationship between the decay rate (G) and the scattering vector squared (q^2) assuming the data goes through (0, 0). The hydrodynamic radius was calculated from the diffusion coefficient using the Stokes–Einstein equation with the refractive index of chlorobenzene (1.5326) and viscosity of chlorobenzene (0.6149 mPa s at 80 °C, 0.6958 mPa s at 65 °C, 0.7938 mPa s at 50 °C, 0.9261 mPa s at 35 °C, and 1.1159 mPa s at 20 °C).

Author contributions

Maged Abdelsamie: conceptualization (lead); investigation (lead); methodology (equal); visualization (supporting); writing – original draft (supporting). Thomas P. Chaney: formal analysis (lead); visualization (lead); methodology (equal); writing – original draft (lead); writing – review and editing (lead); Hongping Yan: investigation (supporting); writing – review and editing (supporting). Sebastian A. Schneider: investigation (supporting); visualization (supporting); writing – review and editing (supporting). Alperen Ayhan: investigation (supporting) writing – original draft (supporting); Enrique D. Gomez: supervision (supporting); funding acquisition (equal). John R. Reynolds supervision (supporting); funding acquisition (equal). Michael F. Toney: supervision (lead); funding acquisition (equal); writing – review and editing (supporting).

Conflicts of interest

There are no conflicts to declare.

Acknowledgements

We thank Dr Bing Xu for the synthesis of the PffBT4T-2OD and PffBT3T-2OD polymers used in this study. We thank the Office of Naval Research for support through the Center for Self-Assembled Organic Electronics (SOE), grant N00014-19-1-2453 (TPC, SAS, MFT, IAA, EDG) and grant N00014-21-1-2087 (JRR). Use of the Stanford Synchrotron Radiation Lightsource (SSRL), SLAC National Accelerator Laboratory, is supported the US DOE, Office of Science, Office of Basic Energy Sciences under Contract DE-AC02-76SF00515.

References

1 A. Guerrero and G. Garcia-Belmonte, Recent Advances to Understand Morphology Stability of Organic Photovoltaics, *Nano-Micro Lett.*, 2017, **9**(1), 10, DOI: 10.1007/s40820-016-0107-3.

2 H. Gaspar, F. Figueira, L. Pereira, A. Mendes, J. Viana and G. Bernardo, *Materials*, 2018, **11**, 2560.

3 S. M. Menke and R. J. Holmes, Exciton Diffusion in Organic Photovoltaic Cells, *Energy Environ. Sci.*, 2014, **7**(2), 499–512, DOI: 10.1039/C3EE42444H.

4 Y. Yi, V. Coropceanu and J.-L. Brédas, Exciton-Dissociation and Charge-Recombination Processes in Pentacene/C60 Solar Cells: Theoretical Insight into the Impact of Interface Geometry, *J. Am. Chem. Soc.*, 2009, **131**(43), 15777–15783, DOI: 10.1021/ja905975w.

5 Y. Diao, Y. Zhou, T. Kurosawa, L. Shaw, C. Wang, S. Park, Y. Guo, J. A. Reinspach, K. Gu, X. Gu, B. C. K. Tee, C. Pang, H. Yan, D. Zhao, M. F. Toney, S. C. B. Mannsfeld and Z. Bao, Flow-Enhanced Solution Printing of All-Polymer Solar Cells, *Nat. Commun.*, 2015, **6**(1), 7955, DOI: 10.1038/ncomms8955.

6 C. McDowell, M. Abdelsamie, M. F. Toney and G. C. Bazan, Solvent Additives: Key Morphology-Directing Agents for Solution-Processed Organic Solar Cells, *Adv. Mater.*, 2018, **30**(33), 1707114, DOI: 10.1002/adma.201707114.

7 F. Panzer, H. Bässler and A. Köhler, Temperature Induced Order–Disorder Transition in Solutions of Conjugated Polymers Probed by Optical Spectroscopy, *J. Phys. Chem. Lett.*, 2017, **8**(1), 114–125, DOI: 10.1021/acs.jpclett.6b01641.

8 A. Wadsworth, M. Moser, A. Marks, M. S. Little, N. Gasparini, C. J. Brabec, D. Baran and I. McCulloch, Critical Review of the Molecular Design Progress in Non-Fullerene Electron Acceptors towards Commercially Viable Organic Solar Cells, *Chem. Soc. Rev.*, 2019, **48**(6), 1596–1625, DOI: 10.1039/C7CS00892A.

9 T. Heumueller, W. R. Mateker, I. T. Sachs-Quintana, K. Vandewal, J. A. Bartelt, T. M. Burke, T. Ameri, C. J. Brabec and M. D. McGehee, Reducing Burn-in Voltage Loss in Polymer Solar Cells by Increasing the Polymer Crystallinity, *Energy Environ. Sci.*, 2014, **7**(9), 2974–2980, DOI: 10.1039/C4EE01842G.

10 H. Zhao, H. B. Naveed, B. Lin, X. Zhou, J. Yuan, K. Zhou, H. Wu, R. Guo, M. A. Scheel, A. Chumakov, S. V. Roth, Z. Tang, P. Müller-Buschbaum and W. Ma, Hot Hydrocarbon-Solvent Slot-Die Coating Enables High-Efficiency Organic Solar Cells with Temperature-Dependent Aggregation Behavior, *Adv. Mater.*, 2020, **32**(39), 2002302, DOI: 10.1002/adma.202002302.

11 H. Hu, P. C. Y. Chow, G. Zhang, T. Ma, J. Liu, G. Yang and H. Yan, Design of Donor Polymers with Strong Temperature-Dependent Aggregation Property for Efficient Organic Photovoltaics, *Acc. Chem. Res.*, 2017, **50**(10), 2519–2528, DOI: 10.1021/acs.accounts.7b00293.

12 X. Yi, Z. Peng, B. Xu, D. Seyitliyev, C. H. Y. Ho, E. O. Danilov, T. Kim, J. R. Reynolds, A. Amassian, K. Gundogdu, H. Ade and F. So, Critical Role of Polymer Aggregation and Miscibility in Nonfullerene-Based Organic Photovoltaics, *Adv. Energy Mater.*, 2020, **10**(8), 1902430, DOI: 10.1002/aenm.201902430.

13 Y. Liu, J. Zhao, Z. Li, C. Mu, W. Ma, H. Hu, K. Jiang, H. Lin, H. Ade and H. Yan, Aggregation and Morphology Control Enables Multiple Cases of High-Efficiency Polymer Solar Cells, *Nat. Commun.*, 2014, **5**(1), 5293, DOI: 10.1038/ncomms6293.

14 J. L. Hernandez, N. Deb, R. M. W. Wolfe, C. K. Lo, S. Engmann, L. J. Richter and J. R. Reynolds, Simple Transfer from Spin Coating to Blade Coating through Processing Aggregated Solutions, *J. Mater. Chem. A*, 2017, **5**(39), 20687–20695, DOI: 10.1039/C7TA05214F.

15 N. D. Eastham, A. S. Dudnik, T. J. Aldrich, E. F. Manley, T. J. Fauvell, P. E. Hartnett, M. R. Wasielewski, L. X. Chen, F. S. Melkonyan, A. Facchetti, R. P. H. Chang and T. J. Marks, Small Molecule Acceptor and Polymer Donor Crystallinity and Aggregation Effects on Microstructure Templating: Understanding Photovoltaic Response in Fullerene-Free Solar Cells, *Chem. Mater.*, 2017, **29**(10), 4432–4444, DOI: 10.1021/acs.chemmater.7b00964.

16 Y. Wu, S. Schneider, C. Walter, A. H. Chowdhury, B. Bahrami, H.-C. Wu, Q. Qiao, M. F. Toney and Z. Bao, Fine-Tuning Semiconducting Polymer Self-Aggregation and Crystallinity Enables Optimal Morphology and High-Performance Printed All-Polymer Solar Cells, *J. Am. Chem. Soc.*, 2020, **142**(1), 392–406, DOI: 10.1021/jacs.9b10935.

17 B. McCulloch, V. Ho, M. Hoarfrost, C. Stanley, C. Do, W. T. Heller and R. A. Segalman, Polymer Chain Shape of Poly(3-Alkylthiophenes) in Solution Using Small-Angle Neutron Scattering, *Macromolecules*, 2013, **46**(5), 1899–1907, DOI: 10.1021/ma302463d.

18 K. Schmidt, C. J. Tassone, J. R. Niskala, A. T. Yiu, O. P. Lee, T. M. Weiss, C. Wang, J. M. J. Fréchet, P. M. Beaujuge and M. F. Toney, A Mechanistic Understanding of Processing Additive-Induced Efficiency Enhancement in Bulk Heterojunction Organic Solar Cells, *Adv. Mater.*, 2014, **26**(2), 300–305, DOI: 10.1002/adma.201303622.

19 M. A. Brady, S.-Y. Ku, L. A. Perez, J. E. Cochran, K. Schmidt, T. M. Weiss, M. F. Toney, H. Ade, A. Hexemer, C. Wang, C. J. Hawker, E. J. Kramer and M. L. Chabinyc, Role of Solution Structure in Self-Assembly of Conjugated Block

Copolymer Thin Films, *Macromolecules*, 2016, **49**(21), 8187–8197, DOI: 10.1021/acs.macromol.6b01686.

20 Z. Hamid, A. Wadsworth, E. Rezasoltani, S. Holliday, M. Azzouzi, M. Neophytou, A. A. Y. Guilbert, Y. Dong, M. S. Little, S. Mukherjee, A. A. Herzing, H. Bristow, R. J. Kline, D. M. DeLongchamp, A. A. Bakulin, J. R. Durrant, J. Nelson and I. McCulloch, Influence of Polymer Aggregation and Liquid Immiscibility on Morphology Tuning by Varying Composition in PffBT4T-2DT/Nonfullerene Organic Solar Cells, *Adv. Energy Mater.*, 2020, **10**(8), 1903248, DOI: 10.1002/aenm.201903248.

21 B. Xu, I. Pelse, S. Agarkar, S. Ito, J. Zhang, X. Yi, Y. Chujo, S. Marder, F. So and J. R. Reynolds, Randomly Distributed Conjugated Polymer Repeat Units for High-Efficiency Photovoltaic Materials with Enhanced Solubility and Processability, *ACS Appl. Mater. Interfaces*, 2018, **10**(51), 44583–44588, DOI: 10.1021/acsami.8b15522.

22 M. P. Aplan, C. Grieco, Y. Lee, J. M. Munro, W. Lee, J. L. Gray, Z. D. Seibers, B. Kuei, J. H. Litofsky, S. M. Kilbey, Q. Wang, I. Dabo, J. B. Asbury and E. D. Gomez, Conjugated Block Copolymers as Model Systems to Examine Mechanisms of Charge Generation in Donor–Acceptor Materials, *Adv. Funct. Mater.*, 2019, **29**(1), 1804858, DOI: 10.1002/adfm.201804858.

23 J. Ilavsky and P. R. Jemian, Irena: Tool Suite for Modeling and Analysis of Small-Angle Scattering, *J. Appl. Crystallogr.*, 2009, **42**(2), 347–353, DOI: 10.1107/S0021889809002222.

24 G. Beaucage, Approximations Leading to a Unified Exponential/Power-Law Approach to Small-Angle Scattering, *J. Appl. Crystallogr.*, 1995, **28**(6), 717–728, DOI: 10.1107/S0021889895005292.

25 G. Beaucage, Small-Angle Scattering from Polymeric Mass Fractals of Arbitrary Mass-Fractal Dimension, *J. Appl. Crystallogr.*, 1996, **29**(2), 134–146.

26 J. T. Rogers, K. Schmidt, M. F. Toney, G. C. Bazan and E. J. Kramer, Time-Resolved Structural Evolution of Additive-Processed Bulk Heterojunction Solar Cells, *J. Am. Chem. Soc.*, 2012, **134**(6), 2884–2887, DOI: 10.1021/ja2104747.

27 F. Liu, Y. Gu, C. Wang, W. Zhao, D. Chen, A. L. Briseno and T. P. Russell, Efficient Polymer Solar Cells Based on a Low Bandgap Semi-Crystalline DPP Polymer-PCBM Blends, *Adv. Mater.*, 2012, **24**(29), 3947–3951, DOI: 10.1002/adma.201200902.

28 Z. Peng, L. Ye and H. Ade, Understanding, Quantifying, and Controlling the Molecular Ordering of Semiconducting Polymers: From Novices to Experts and Amorphous to Perfect Crystals, *Mater. Horiz.*, 2022, DOI: 10.1039/D0MH00837K.

29 B. Hammouda, Analysis of the Beaucage Model, *J. Appl. Crystallogr.*, 2010, **43**(6), 1474–1478, DOI: 10.1107/S0021889810033856.

30 R. Xie, A. R. Weisen, Y. Lee, M. A. Aplan, A. M. Fenton, A. E. Masucci, F. Kempe, M. Sommer, C. W. Pester, R. H. Colby and E. D. Gomez, Glass Transition Temperature from the Chemical Structure of Conjugated Polymers, *Nat. Commun.*, 2020, **11**(1), 893, DOI: 10.1038/s41467-020-14656-8.

31 F. L. Lee, A. Barati Farimani, K. L. Gu, H. Yan, M. F. Toney, Z. Bao and V. S. Pande, Solution-Phase Conformation and Dynamics of Conjugated Isoindigo-Based Donor–Acceptor Polymer Single Chains, *J. Phys. Chem. Lett.*, 2017, **8**(22), 5479–5486, DOI: 10.1021/acs.jpclett.7b02360.

32 C. C. Hua, C. J. Lin, Y. H. Wen and S. A. Chen, Stabilization of Bulk Aggregation State in Semiconducting Polymer Solutions, *J. Polym. Res.*, 2011, **18**(4), 793–800, DOI: 10.1007/s10965-010-9476-3.

33 K. Schillen, W. Brown and C. Konak, Aggregation of a Poly(Ethylene Oxide)-Poly(Propylene Oxide)-Poly(Ethylene Oxide) Triblock Copolymer in Aqueous Solution Studied Using Rayleigh-Brillouin and Dynamic Light Scattering, *Macromolecules*, 1993, **26**(14), 3611–3614, DOI: 10.1021/ma00066a020.

34 B. Xu, I. Pelse, S. Agarkar, S. Ito, J. Zhang, X. Yi, Y. Chujo, S. Marder, F. So and J. R. Reynolds, Randomly Distributed Conjugated Polymer Repeat Units for High-Efficiency Photovoltaic Materials with Enhanced Solubility and Processability, *ACS Appl. Mater. Interfaces*, 2018, **10**(51), 44583–44588, DOI: 10.1021/acsami.8b15522.

35 G. Pirotte, S. Agarkar, B. Xu, J. Zhang, L. Lutsen, D. Vanderzande, H. Yan, P. Pollet, J. R. Reynolds, W. Maes and S. R. Marder, Molecular Weight Tuning of Low Bandgap Polymers by Continuous Flow Chemistry: Increasing the Applicability of PffBT4T for Organic Photovoltaics, *J. Mater. Chem. A*, 2017, **5**(34), 18166–18175, DOI: 10.1039/C7TA05627C.

36 J. Ilavsky, Nika: Software for Two-Dimensional Data Reduction, *J. Appl. Crystallogr.*, 2012, **45**(2), 324–328, DOI: 10.1107/S0021889812004037.

37 S. D. Oosterhout, V. Savikhin, J. Zhang, Y. Zhang, M. A. Burgers, S. R. Marder, G. C. Bazan and M. F. Toney, Mixing Behavior in Small Molecule:Fullerene Organic Photovoltaics, *Chem. Mater.*, 2017, **29**(7), 3062–3069, DOI: 10.1021/acs.chemmater.7b00067.